Tanshinone IIA suppresses cancer metastasis by modulating tumor cell-platelet-endothelial cell interactions

JUDAN XU[1,2*], LIN LUO[2,3*], FEIYANG LI[3,4], SIYING WANG[1,2], CHENGBIN FU[5], GUIHUA WANG[1], YANHONG WANG[1] and YUSHENG LU[2]

[1]Heilongjiang Provincial Key Laboratory of Environmental Microbiology and Recycling of Argo-Waste in Cold Region, College of Life Science and Biotechnology, Heilongjiang Bayi Agricultural University, Daqing, Heilongjiang 163319, P.R. China; [2]Fuzhou Institute of Oceanography, Fujian-Taiwan-Hongkong-Macao Science and Technology Cooperation Base of Intelligent Pharmaceutics, College of Material and Chemical Engineering, Minjiang University, Fuzhou, Fujian 350108, P.R. China; [3]College of Chemistry and Chemical Engineering, Fuzhou University, Fuzhou, Fujian 350116, P.R. China; [4]Precision Pharmacy and Drug Development Center, Department of Pharmacy, Tangdu Hospital, Air Force Medical University, Xi'an, Shaanxi 710038, P.R. China; [5]Department of Breast Surgery, Fujian Medical University Union Hospital, Fujian Medical University, Fuzhou, Fujian 350001, P.R. China

Received January 23, 2026; Accepted May 15, 2026

DOI: 10.3892/ol.2026.15694

Abstract. Hematogenous metastasis is a major cause of cancer-related mortality and depends on coordinated interactions between circulating tumor cells, platelets and vascular endothelial cells. Targeting this metastatic microenvironment represents a promising strategy to limit tumor dissemination. Tanshinone IIA (Tan IIA), a bioactive compound derived from *Salvia miltiorrhiza*, has anti-tumor activity, however, its effects on tumor cell-platelet-endothelial interactions during metastasis remain incompletely understood. In the present study, Tan IIA was evaluated at low, non-cytotoxic concentrations to assess its influence on metastatic processes rather than direct tumor cell killing. In assessments of cell viability and the cell cycle, Tan IIA exhibited minimal effects on the viability of tumor and endothelial cells, while significantly suppressing tumor cell migration and invasion *in vitro*. Mechanistically, Tan IIA decreased CD29 expression on tumor cells, inhibited platelet activation, as indicated by decreased P-selectin expression, and attenuated tumor cell-platelet aggregate formation. Tan IIA diminished TNF-α-induced upregulation of endothelial adhesion molecules intercellular adhesion molecule-1 and E-selectin, resulting in decreased tumor cell adhesion to endothelial monolayers by inhibiting the NF-κB signaling pathway. These coordinated effects resulted in a significant reduction in pulmonary metastatic burden and prolonged survival in mouse models of hematogenous metastasis, without evidence of overt systemic toxicity. Collectively, these findings indicated that Tan IIA suppresses metastatic dissemination primarily by modulating interactions between tumor cells, platelets and endothelial cells, highlighting its potential as a pharmacological agent targeting the metastatic microenvironment.

Correspondence to: Mr. Feiyang Li, Precision Pharmacy and Drug Development Center, Department of Pharmacy, Tangdu Hospital, Air Force Medical University, Pharmacy Office Building, 5FL Xinshi Road, Xi'an, Shaanxi 710038, P.R. China
E-mail: 879577047@qq.com

Professor Yusheng Lu, Fuzhou Institute of Oceanography, Fujian-Taiwan-Hongkong-Macao Science and Technology Cooperation Base of Intelligent Pharmaceutics, College of Material and Chemical Engineering, Minjiang University, Kechuang Building, 3FL Xiyuangong Road, Fuzhou, Fujian 350108, P.R. China
E-mail: yushenglu@mju.edu.cn

*Contributed equally

Key words: tanshinone IIA, cancer metastasis, circulating tumor cell, platelet-tumor cell interaction, endothelial adhesion, cancer microenvironment

Introduction

Most cancer-related deaths (~90%) are caused by metastatic cancer (1), which has become a notable obstacle to effective cancer treatment. Metastasis begins when malignant cells detach from the primary tumor, disseminate through the lymphatic system, bloodstream or body cavities and colonize distant organs (2,3). This multistep process is influenced by the cancer microenvironment, which can either restrain or promote the metastatic potential of tumor cells (4). Once tumor cells enter the circulation, they are referred to as circulating tumor cells (CTCs), which serve a key role in the establishment of distant metastases (5).

Although platelets are primarily responsible for maintaining hemostasis, growing evidence indicates they actively participate in cancer progression (6,7). CTCs can activate platelets and form tumor cell-platelet aggregates, which shield tumor cells from immune surveillance and enhance their survival in the bloodstream. In addition, activated platelets adhere to vascular endothelial cells, facilitating the attachment of these aggregates to the vessel wall. This promotes tumor

cell extravasation through the endothelial barrier and basement membrane, leading to the formation of secondary tumors (8). Consequently, interactions between CTCs and platelets are a critical driving force in cancer metastasis (7).

The vascular endothelium also serves a key role in the process of tumor metastasis. During CTC adhesion, endothelial cells upregulate surface adhesion molecules in response to stimulation, thereby strengthening tumor cell attachment (9). This initiates a cascade of events such as endothelial cytoskeletal rearrangement, increased endothelial permeability and basement membrane degradation, all of which promotes tumor cell transmigration and metastatic colonization. Our previous studies demonstrated that adhesion of CTCs to the vascular endothelium is a crucial early step in distant metastasis and that disrupting this interaction can markedly suppress metastatic spread (4,5,10). Despite these findings, effective clinical strategies targeting CTC adhesion and metastasis remain limited, highlighting the need to identify novel therapeutic agents and targets.

Salvia miltiorrhiza, a traditional Chinese herb first documented in Shennong's Classic of Herbal Medicine, has been used to promote blood circulation (11). Clinically, it has therapeutic benefits in the treatment of stroke (12), cardiovascular disease and osteoporosis (13). Tanshinone IIA (Tan IIA), a major bioactive compound derived from *S. miltiorrhiza*, exhibits a wide range of pharmacological activities, including anti-inflammatory, antioxidant and antitumor effects (14-19). Tan IIA is applied in the management of cardiovascular and cerebrovascular disorders (20) due to its vasodilatory, anticoagulant, antithrombotic and endothelial-protective properties (21-25).

Tan IIA can reduce vascular oxidative stress, inhibit platelet aggregation and protect endothelial function (26), suggesting its potential to modulate platelet-endothelium interactions. Tan IIA has also demonstrated therapeutic potential in metabolic disorders such as diabetes (27,28). Tan IIA exerts antitumor effects across multiple cancer types (29,30). Tan IIA has been shown to suppress tumor cell proliferation, migration and metastasis by regulating cytoskeletal dynamics (31), inhibiting oncogenic signaling pathways (32) and inducing ferroptosis (33). These effects have been reported in liver, lung, breast, prostate (34) and colorectal cancer (35-37). However, the role of Tan IIA in regulating interactions between CTCs, platelets and endothelial cells remains poorly understood.

The present study investigated the effects of Tan IIA at low concentrations on platelets and endothelial cells using both *in vivo* and *in vitro* models. The aim was to elucidate how Tan IIA modulates platelet-tumor cell interactions and tumor cell adhesion to the vascular endothelium, thereby providing mechanistic insight into its potential to prevent CTC-mediated metastasis.

Materials and methods

Cell culture. The human non-small cell lung cancer cell A549, human breast cancer MCF-7 and mouse breast cancer 4T1 cells were obtained from the Cell Bank of the Chinese Academy of Sciences. A549 cells were cultured in RPMI-1640 medium (cat. no. SH30027.01; Hyclone; Cytiva) supplemented with 10% fetal bovine serum (FBS; cat. no. A5256701; Gibco; Thermo Fisher Scientific, Inc.), 100 U/ml penicillin and 100 μg/ml streptomycin. MCF-7 and 4T1 cells were cultured in high-glucose DMEM (cat. no. SH30243.01; Hyclone; Cytiva) supplemented with 10% FBS, 100 U/ml penicillin and 100 μg/ml streptomycin. Human umbilical vein endothelial cells (HUVECs) were isolated as previously described (38) and cultured in 1% gelatin-coated flasks using endothelial cell medium (cat. no. #1001; ScienCell Research Laboratories, Inc.) supplemented with 5% FBS, 100 μg/ml endothelial cell growth supplement (cat. no. #1052; ScienCell Research Laboratories, Inc.), 100 U/ml penicillin and 100 μg/ml streptomycin. All cells were maintained at 37˚C in a humidified incubator containing 5% CO_2. Cells were harvested using 0.25% trypsin prior to experiments. HUVECs were used within six passages.

Drug preparation. Tan IIA (purity, ≥98%, cat. no. S107694; lot no. K2208491) was obtained from Shanghai Aladdin Biochemical Technology Co., Ltd. For the *in vitro* experiments, Tan IIA was dissolved in DMSO to a stock solution of 40 mM, filtered, stored at 4˚C and diluted with normal saline when used.

Cell viability assay. The cytotoxicity of Tan IIA was evaluated using the MTT assay as previously described (4). Briefly, MCF-7, A549 and HUVEC cells were seeded into 96-well plates at a density of $1x10^4$ cells per well and incubated at 37˚C for 24 h. The cells were treated with medium containing various concentrations (0, 5, 10 and 20 μM) of Tan IIA at 37˚C for 24 h. MTT solution was added, followed by incubation for 4 h at 37˚C. The medium was removed and formazan crystals were dissolved in 100 μl DMSO. Absorbance was measured at 570 nm using a microplate reader (Tecan Group Ltd.; M200 PRO). All absorbance values were normalized to blank wells containing culture medium and MTT reagent only, which served as the zero metabolic activity baseline. Cell viability was expressed as a percentage relative to untreated controls.

Cell cycle and apoptosis assay. A549 and HUVEC cells in logarithmic growth phase were treated with Tan IIA (0, 5, 10 and 20 μM) at 37˚C for 24 h and collected using trypsin without EDTA. For cell cycle analysis, A549 cells were fixed in 70% ethanol at 4˚C for 12 h, treated with RNase and stained with PI. For apoptosis analysis (early and late apoptotic cells), treated cells (A549 and HUVEC cells) were resuspended in binding buffer and stained with 5 μl of Annexin V-FITC and 5 μl of PI for 15 min in the dark at room temperature, followed by the addition of 0.5 ml PBS. Cell cycle and apoptosis were detected by flow cytometry with a BD FACSAria (BD Biosciences) and analyzed by FlowJo software (version number 10.8.1; BD Biosciences).

Wound healing assay. Cell migration was evaluated using a wound healing assay. A549 cells were seeded into 12-well plates ($2x10^5$ cells/well) and allowed to form a confluent (80-90%) monolayer. A linear scratch was created using a pipette tip and detached cells were removed with serum-free RPMI-1640. Cells were incubated in RPMI-1640 containing 1% FBS and Tan IIA at the indicated concentrations (0, 5, 10 and 20 μM).

Images were captured at 0 and 24 h using a light microscope. The migration of the cells was assessed by measuring the width of the wound area.

Cell invasion assay. Cell invasion assay was assessed using Matrigel-coated Transwell chambers (Corning, Inc.; 8 μm pore size) as previously described (39). The membrane was coated with 0.5% Matrigel overnight at 37˚C. A549 cells ($4x10^4$) were seeded into the upper chamber in serum-free RPMI-1640 medium containing Tan IIA (0, 10 and 20 μM), while the lower chamber contained RPMI-1640 medium with 10% FBS. After 24 h of incubation at 37˚C in a cell culture incubator, non-invading cells were removed and invading cells were fixed with 4% paraformaldehyde for 20 min at 4˚C and stained with 0.1% crystal violet at room temperature for 30 min. Images of the stained cells were captured using a light microscope. The invasive ability was quantified by counting the number of cells that had penetrated through the membrane and analyzed using ImageJ software (version number 1.54p; National Institutes of Health).

Flow cytometric analysis of cell adhesion molecules. A549 cells were treated with different concentrations of Tan IIA (0, 5, 10 and 20 μM) at 37˚C for 24 h, and HUVECs were treated with 0, 5 and 10 μM of Tan IIA at 37˚C for 24 h. Prior to treatment, HUVECs were stimulated with TNF-α (10 ng/ml) at 37˚C for 4 h (negative control, HUVECs without TNF-α). Subsequently, the cells were harvested, resuspended in PBS and incubated in the dark at room temperature for 10 min with 10 μl antibodies as follows: Anti-CD29 (PE-labeled, cat. no. 303004) for A549 cells and anti-ICAM (cat. no. 353112) or anti-E-selectin (both APC-labeled, cat. no. 336011) (all 1:100, all Biolegend, Inc.) for HUVECs. After washing with PBS buffer, cells were analyzed using a BD FACSAria and FlowJo software.

Platelet activity assay. Blood was collected from 5 volunteers at the Blood Bank of Fujian Medical University Union Hospital (Fuzhou, China) between May and October 2023. The study included 2 men and 3 women, aged 20-40 years. The inclusion criteria were as follows: i) Normal platelet aggregation function; ii) normal coagulation parameters and other complete blood count indices; and iii) no use of any anticoagulants for 2 weeks prior to blood collection. All participants provided written informed consent before sample collection, explicitly agreeing to the use of their blood samples for the present study. The study was approved by the Ethics Committee of Fujian Medical University Union Hospital (Fuzhou, China; approval no.2022KJT046) and was conducted in compliance with the Declaration of Helsinki. All patients provided written informed consent to participate.

Fresh blood (1.8 ml) was added to a centrifuge tube containing 0.2 ml sodium citrate anticoagulant. After centrifugation at 2,000 x g for 10 min at room temperature, the upper layer of the supernatant was collected to obtain platelet-rich plasma. The platelet-rich plasma was centrifuged at 15,00 x g for 15 min at room temperature and the lower pellet was collected as the platelet precipitate, yielding a platelet concentration of ~$2x10^6$ platelets/μl. The procedure was completed rapidly to prevent platelet aggregation. To investigate the effect of Tan IIA on platelet activity, the platelet pellet (10 μl) was resuspended in 1 ml PBS. Platelets were activated with ADP (20 μM) while being treated with varying concentrations of Tan IIA (0, 1, 5 and 10 μM). The mixture was incubated at 37˚C for 5 min. Thereafter, 20 μl P-selectin (1:100, PE-labeled; cat. no. 148306; Biolegend, Inc.) antibody was added to each tube containing 200 μl of platelet suspension, followed by incubation in the dark at 37˚C for 15 min. The effect of Tan IIA on platelet activity was analyzed by flow cytometry with a BD FACSAria and the resulting data were processed using FlowJo software.

Adhesion of cancer to endothelial cells. Gelatin-coated 24-well plates (gelatin coating was performed by incubation at 37˚C for 1 h) were seeded with HUVECs at a density of $2x10^5$ cells per well to form confluent (80-90%) monolayers, which were pretreated with TNF-α (10 ng/ml) at 37˚C for 4 h. A group without TNF-α was set as the blank control. A549 cells suspension at ~$6x10^5$ cells/ml treated with Tan IIA (0, 5, 10, 20 μM) at 37˚C and labeled with Rhodamine-123 (10 μl; 15 min) were added and co-cultured with HUVECs at 37˚C for 1 h. After washing away non-adherent cells with PBS, fluorescence microscopy images were captured in 12 randomly selected fields of view/well. Adhesion was quantified as a percentage relative to control.

To assess platelet-mediated adhesion, A549 cell suspension (~$6x10^5$ cells/ml) were treated with Tan IIA (0, 5, 10 and 20 μM) at 37˚C and labeled with 10 μl Rhodamine-123 stain for 15 min. After adding 10 μl platelet-rich plasma, the cell mixture was co-incubated with HUVECs at a density of $2x10^5$ cells per well (pretreated with 10 ng/ml TNF-α for 4 h) at 37˚C for 1 h, with the simultaneous addition of ADP (20 μM) to activate platelets. A group without TNF-α stimulation was used as the blank control. Adhesion was quantified as a percentage relative to control.

Cancer cell-platelet aggregation assay. The platelet cloaking of cancer cells was performed as previously described (4). Briefly, A549 cells were harvested and suspended in PBS at a density of $2x10^6$ cells/ml. Tan IIA (0, 5, 10 and 20 μM) and A549 cells ($2x10^5$ cells) were added to 100 μl PBS containing suspended platelets ($2x10^8$ cells/ml) in centrifuge tubes, followed by the addition of ADP (20 μM) to stimulate platelet activation. After 5 min incubation at 25˚C, 20 μl each mouse anti-human CD61 (FITC-labeled, cat. no. 104306) and CD326 (PE-labeled, cat. no. 324205) (both 1:100, Biolegend, Inc.) were added to the tubes. The mixture was incubated for 20 min at 4˚C in the dark, followed by the addition of 1 ml ice-cold 1% paraformaldehyde for fixation at 4˚C for 30 min. A549 cells cloaked by platelets were identified by flow cytometry with a BD FACSAria; $CD61^+CD326^+$ cancer cells were considered platelet-cloaked cancer cells. The data were analyzed using FlowJo software.

Fluorescence microscopy of platelet-cancer cell interaction. The adhesion of platelets to tumor cells following Tan IIA (0, 5, 10, and 20 μM) treatment was visualized using a confocal fluorescence microscope (Leica GmbH; STELLARIS 5). Suspended platelets (10 μl at a density of ~$2x10^6$ platelets/μl) were collected and stained with 5 μM 5-(and-6)-carboxyfluorescein diacetate N-succinimidyl ester (cat. no. 21888;

Sigma-Aldrich; Merck KGaA) in PBS for 10 min at 37˚C. The nuclei of A549 cells were stained with DAPI (1 μg/ml in PBS) for 15 min at 25˚C in the dark and the cell membranes were stained with 2 μM PKH26 Red Fluorescent Cell Linker (cat. no. MINI26-1KT; Sigma-Aldrich; Merck KGaA) for 15 min at 25˚C in the dark. Subsequently, the stained platelets and tumor cells were co-cultured for 10 min at 25˚C in the dark. After co-culture, unattached platelets were removed by washing with PBS and the platelet-tumor aggregates were transferred to confocal dishes for incubation at 37˚C for 4 h. Finally, 12 randomly selected fields of view/dish were observed using a confocal microscope. The number of platelets adhering to tumor cells was quantified by ImageJ software.

Western blotting. Western blotting was performed to detect the effect of Tan IIA at safe concentrations (0, 5 and 10 μM) at 37˚C for 24 h on the NF-κB signaling pathway in HUVECs. Whole-cell lysates were from HUVECs prepared using RIPA Buffer (cat. no. WB3100; Suzhou Xinsaimei Biotechnology Co., Ltd.) with 1% protease/phosphatase inhibitors on ice for 30 min, followed by centrifugation at 12,000 x g for 20 min at 4˚C. Protein concentration was determined using the BCA method. Proteins (10 μg/lane) were separated using 4-12% gradient precast gels according to their molecular sizes and transferred to PVDF membranes. Membranes were blocked with 5% skimmed milk and 5% BSA (cat. no. T50811010260; Beijing Dingguo Changsheng Biotechnology Co., Ltd.) at room temperature for 90 min and incubated with primary antibodies at 4˚C overnight. After washing with TBST (0.1% Tween) four times, 5 min each, the membranes were incubated with horseradish peroxidase-conjugated secondary antibodies (1:5,000; cat. no. 511203; Zenbio; Chengdu Zhengneng Biotechnology Co., Ltd.) for 1 h at room temperature. Signals were detected using an ECL substrate (NcmECL Ultra; cat. no. P10300; Suzhou Xinsaimei Biotechnology Co., Ltd.) and a chemiluminescence imaging system (ChemiDoc™ MP; Bio-Rad Laboratories, Inc.). The following primary antibodies were used: GAPDH (1:10,000; cat. no. A19056; ABclonal Biotech Co., Ltd.), NF-κB p65 (cat. no. R25149), phosphorylated (p-) NF-κB p65 (cat. no. 310013), IκB-α (cat. no. R23322), p-IκB-α (cat. no. 340776), IKK-α/β (cat. no. R24676) and p-IKK-α/β (all 1:1,000; cat. no. 530546; all Zenbio). Band intensities from three independent experiments were semi-quantified using ImageJ software.

Molecular docking. The 3D structure of Tan IIA was downloaded from the PubChem database (pubchem.ncbi.nlm.nih.gov/) in SDF format. The compound was converted to MOL2 format using PyMOL (version number 3.1.6; Delano Scientific LLC), and its geometric conformation was automatically optimized. The 3D structure of the target protein was retrieved from the Research Collaboratory for Structural Bioinformatics Protein Data Bank (rcsb.org/). The protein structure was processed by removing water molecules, adding hydrogen atoms and checking charge states. Both the ligand (Tan IIA) and the receptor (CD29 and P-selectin) were converted to the PDBQT format using the MGLTools software package (version number 1.5.7; The Scripps Research Institute). Molecular docking was then performed using AutoDock Vina (version number 1.1.2; The Scripps Research Institute) to calculate the binding energies. The best docking pose was selected and visualized using PyMOL.

In vivo assays. All animal procedures were conducted in accordance with the Guide for the Care and Use of Laboratory Animals (National Research Council, 2011) (40). The Laboratory Animal Ethics Committee of Minjiang University (Fuzhou, China) reviewed and approved all animal procedures (approval no. IACUC-MJLAC-2023-020).

Female BALB/c and nude mice (n=110; weight, 20±2 g; age, 6-8 weeks) were obtained from Shanghai SLAC Laboratory Animal Co., Ltd. The animals were acclimatized to the laboratory environment for ≥1 week prior to the start of the experiment. All mice were housed in a specific-pathogen-free facility at the Animal Experiment Center of Minjiang University, with 5 mice/cage under a 12/12-h light/dark cycle at a constant temperature of 23-25˚C and 50-60% relative humidity. They were fed a standard rodent diet and had free access to sterile water, which was replaced daily. The experiment lasted 4-6 weeks.

Animal health and behavior were monitored daily for clinical signs including activity levels, appetite and grooming. Body weights were measured and recorded every 3 days throughout the study. Humane endpoints were as follows: i) Maximum tumor volume >750 mm^3; ii) severe clinical manifestations such as dyspnea or listlessness; and iii) body weight loss >20% of initial body weight. In total, four mice were prematurely euthanized based on tumor volume and clinical manifestations.

To prepare the vehicle, 0.1 g sodium carboxymethyl cellulose (cat. no. C104984; Shanghai Aladdin Biochemical Technology Co., Ltd.) was dissolved in 100 ml double-distilled water to obtain a 0.1% solution. Tan IIA was dissolved in this 0.1% sodium carboxymethyl cellulose solution to prepare Tan IIA solutions at concentrations of 0.1, 1 and 2 mg/100 μl for oral gavage. The anti-metastatic efficacy of Tan IIA was evaluated using three independent mouse cancer models (n=10). For the A549 lung metastasis model, A549 cells in logarithmic growth phase ($1x10^5$ cells in 100 μl per mouse) were injected into the tail vein of nude mice. For the hematogenous metastasis model, 4T1 cells in logarithmic growth phase ($1x10^5$ cells in 100 μl per mouse) were injected via the tail vein of Balb/c mice. For the orthotopic metastasis model, 4T1 cells ($5x10^5$ cells in 100 μl per mouse) were injected into the fourth mammary fat pad of Balb/c mice to establish an orthotopic tumor model that simulates the natural metastatic progression of breast cancer.

In the A549 lung metastasis model, a high-(1 mg/100 μl/day) and low-dose (0.1 mg/100 μl/day) and control group (100 μl 0.1% sodium carboxymethyl cellulose solution) were set up. In the 4T1 breast cancer metastasis model, a high-(2 mg/100 μl/day), medium-(1 mg/100 μl/day) and low-dose (0.1 mg/100 μl/day) and control group (100 μl 0.1% sodium carboxymethyl cellulose solution; vehicle) were established. Mice continued to receive 100 μl Tan IIA solution or vehicle by oral gavage daily for 4-6 weeks. During this period, the physiological status of the mice was observed and recorded. Body weight was measured and recorded for all surviving mice at every 3 days. At the end of the experiment, mice were anesthetized

by inhalation of 3-5% isoflurane in oxygen for induction, followed by maintenance anesthesia with 1-2% isoflurane. Mice were euthanized with a CO_2 displacement rate of 30% of the container volume/min, followed by cervical dislocation. Death was confirmed by cessation of heartbeat and respiration. The lungs were removed fixed in 4% paraformaldehyde at 4˚C overnight, stained with picric acid at room temperature for 72 h and the number of metastatic nodules was assessed under a dissecting microscope. GraphPad Prism software (version number 8.0.2; Dotmatics) was used for analysis.

Statistical analysis. Data are presented as the mean ± standard deviation of ≥3 independent experimental repeats. Statistical analyses were performed using GraphPad Prism. Differences were evaluated by one-way ANOVA followed by Dunnett's post hoc test. $P<0.05$ was considered to indicate a statistically significant difference.

Results

Tan IIA shows weak cytotoxicity toward A549 cells and HUVECs. The present study aimed to identify Tan IIA concentrations that exert minimal direct cytotoxic effects on tumor and endothelial cells, thereby allowing investigation of its effects on metastasis-associated interactions. Viability was assessed in A549, HUVECs and MCF-7 cells following Tan IIA treatment. Cell viability slightly decreased with increasing Tan IIA concentration, however there was no significant difference in any cell line (Fig. 1A). Consistent with these findings, apoptosis analysis showed no significant increase in apoptotic A549 cells following treatment with Tan IIA (Fig. 1B and C). Cell cycle analysis revealed A549 cell cycle arrest at the G2/M phase following treatment with Tan IIA, while the cell cycle distribution of HUVECs did not change significantly (Fig. 1D-G). This supports the selective action of Tan IIA on carcinoma over normal endothelial cells, a key point for its potential as an anti-metastatic agent with a favorable safety profile regarding vascular toxicity.

Tan IIA suppresses migration and invasion of A549 cells. Tumor cell migration and invasion are key steps in metastatic progression. To examine whether Tan IIA affects these processes, wound healing and Transwell invasion assays were performed. In the wound healing assay, A549 cells treated with non-cytotoxic concentrations of Tan IIA (10 and 20 μM) showed significantly decreased migration compared with untreated controls after 24 h, however lower doses of Tan IIA had no significant effect (Fig. 2A and B). Similarly, Tan IIA inhibited A549 cell invasion in a concentration-dependent (Fig. 2C and D). These findings indicated that Tan IIA effectively suppressed both migration and invasion of lung cancer cells independent of overt cytotoxicity.

Tan IIA reduces adhesion molecules expression on tumor cells and endothelial cells. Adhesion between tumor cells, platelets and endothelial cells plays a central role in metastatic dissemination (41-43). The present study examined whether Tan IIA modulates adhesion molecule expression on tumor cells. CD29, a key integrin involved in platelet binding and cell adhesion, was assessed on A549 cells by flow cytometry (44,45). Tan IIA resulted in a concentration-dependent reduction in CD29 expression on the A549 cell surface (Fig. 3A and B). The present study evaluated the effects of Tan IIA on endothelial adhesion molecules. E-selectin and ICAM are inducible adhesion proteins that facilitate tumor cell attachment to activated endothelium (46). Flow cytometric analysis revealed that Tan IIA significantly decreased the surface expression of E-selectin on HUVECs in a concentration-dependent manner; the expression of ICAM-1 on HUVECs was significantly reduced, while no significant difference in ICAM-1 expression was observed between higher Tan IIA doses (Fig. 3C-F). These results suggested that Tan IIA disrupts a metastasis-promoting microenvironment by decreasing adhesion molecule expression on both tumor cells and endothelial cells.

Tan IIA inhibits platelet activation and tumor cell-platelet aggregate formation. Platelet activation and aggregation around CTCs enhance tumor survival and metastatic potential (47). P-selectin is a member of the selectin family of cell adhesion molecules. It is expressed on stimulated endothelial cells and activated platelets, mediating both heterotypic aggregation between activated platelets and cancer cells, as well as the adhesion of cancer cells to stimulated endothelial surfaces (48). To evaluate the effect of Tan IIA on platelet activity, P-selectin expression was measured by flow cytometry. ADP markedly increased P-selectin expression; addition of Tan IIA significantly decreased P-selectin levels in compared with the control (Fig. 4A and B), indicating inhibition of platelet activation.

To assess tumor cell-platelet interactions, platelet cloaking of A549 cells was examined by flow cytometry. Under resting conditions, few A549 cells exhibited platelet binding. Following ADP-induced platelet activation, the proportion of platelet-coated tumor cells increased markedly. Tan IIA significantly decreased platelet adhesion to A549 cells (Fig. 4C and D). These findings indicate that Tan IIA interfered with platelet-tumor cell aggregate formation by suppressing platelet activation. Collectively, these results demonstrated that Tan IIA may limit key steps of CTC-mediated metastasis by inhibiting platelet activation, decreasing tumor cell-platelet aggregation and decreasing adhesion molecule expression (Fig. 4E).

Tan IIA inhibits tumor cell adhesion to endothelial cells. Adhesion of CTCs to the vascular endothelium is a prerequisite for extravasation and metastatic colonization (49). To evaluate whether Tan IIA affected this process, A549 cells treated with Tan IIA were co-cultured with TNF-α-stimulated HUVEC monolayers. Tan IIA significantly decreased the number of tumor cells adhering to endothelial cells in a concentration-dependent manner (Fig. 5A and B). To investigate the role of platelets in this process, a co-culture system incorporating A549 cells, platelets and activated HUVECs was established. In the presence of platelets, Tan IIA inhibited tumor cell adhesion to endothelial cells (Fig. 5C and D). Confocal microscopy confirmed that Tan IIA decreased platelet coverage of tumor cells, resulting in fewer platelet-tumor cell aggregates (Fig. 5E and F). These findings indicate that Tan IIA inhibits platelet-mediated tumor cell adhesion to the endothelium.

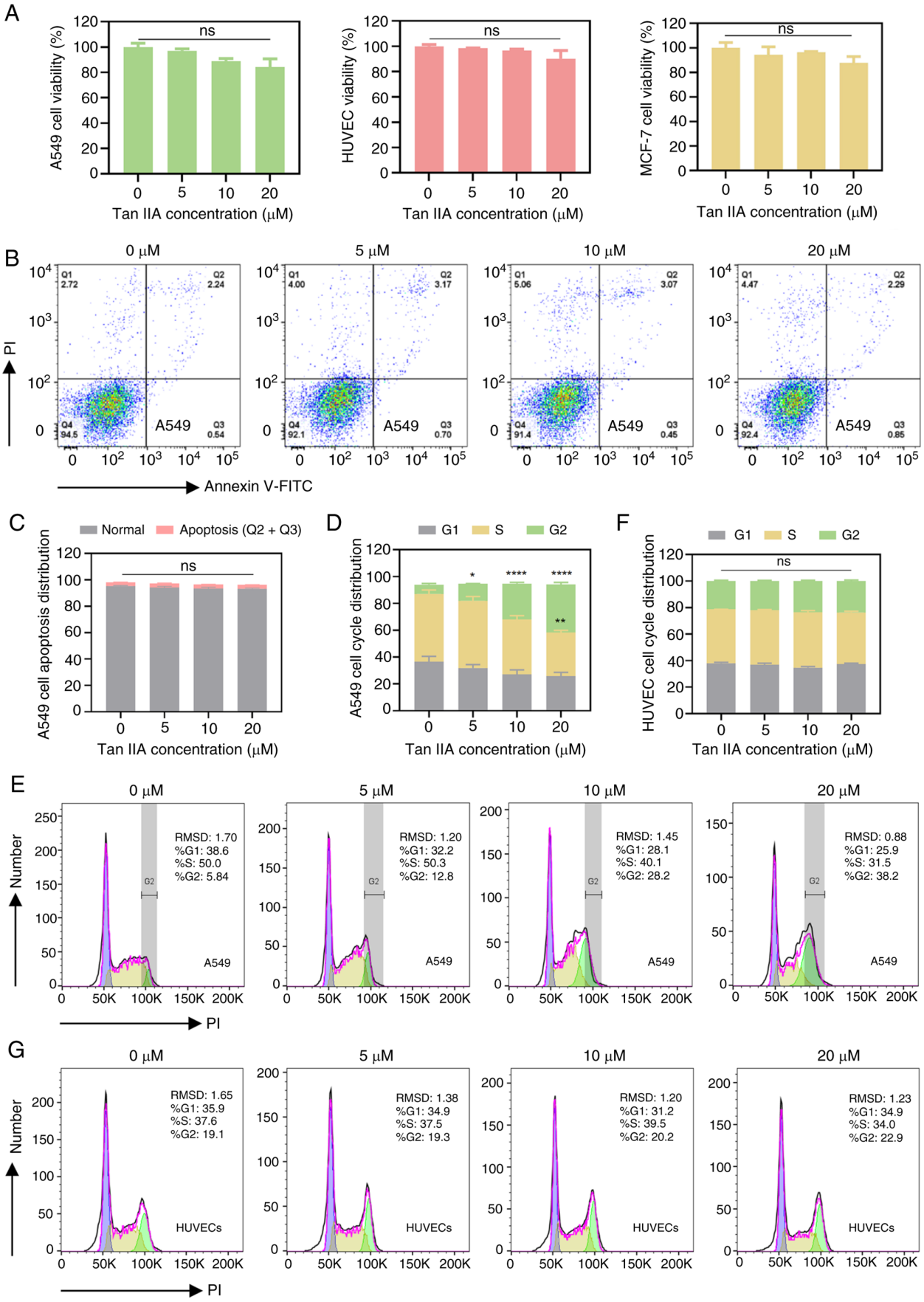

Figure 1. Cytotoxic effects of Tan IIA. (A) Tan IIA exhibited minimal cytotoxicity toward A549 lung and MCF-7 breast cancer cells and HUVECs. (B) Flow cytometric detection of the effects of Tan IIA on A549 cell apoptosis. (C) Quantitative results of A549 cell apoptosis. Apoptosis analysis showed that Tan IIA had no significant effect on A549 cell apoptosis. Following treatment with Tan IIA, quantitative results of (D) A549 cells showed that they were (E) arrested in G2/M phase, and quantitative results of (F) HUVECs showed that their (G) cell cycle distribution did not change significantly. *P<0.05, **P<0.01, ****P<0.0001 vs. 0. Tan IIA, tanshinone IIA; RMSD, root mean square deviation; HUVEC, human umbilical vein endothelial cells; ns, not significant.

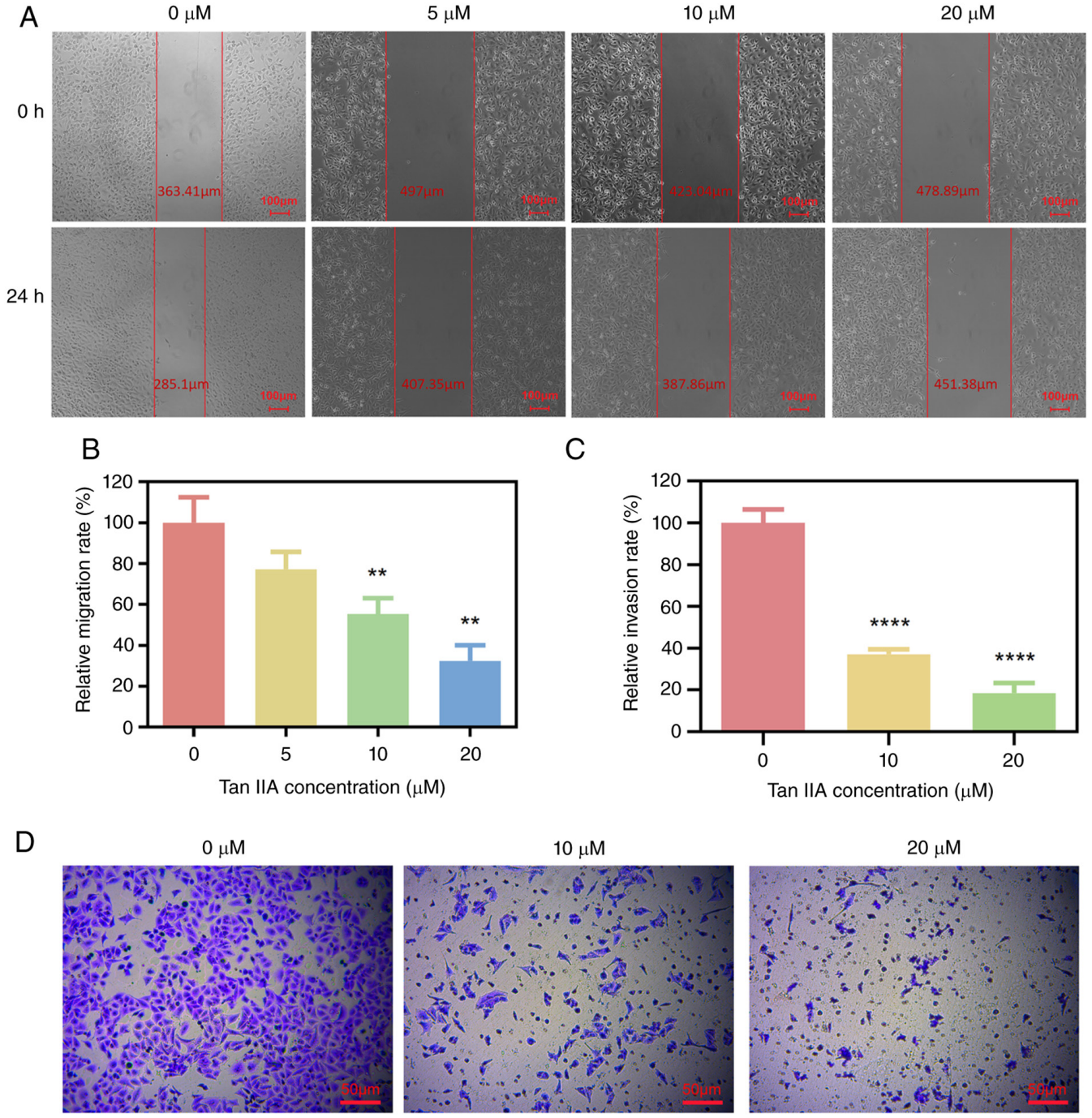

Figure 2. Effects of Tan IIA on tumor cell migration and invasion. (A) Tan IIA significantly inhibited the migratory capacity of A549 cells, as assessed by wound healing assay. (B) Quantitative results of A549 cell migration. (C) Quantitative results of A549 cell invasion which showed that (D) Tan IIA significantly suppressed A549 cells invasion (Matrigel assays). **P<0.01, ****P<0.0001 vs. 0. Tan IIA, tanshinone IIA.

Tan IIA inhibits E-selectin and ICAM expression on HUVECs by regulating the NF-κB signaling pathway. To investigate how Tan IIA affects the expression of the endothelial surface proteins E-selectin and ICAM, the present study examined whether Tan IIA influences the NF-κB signaling pathway in endothelial cells. Endothelial cells were cultured in the presence or absence of TNF-α stimulation. Western blotting was performed to evaluate the effect of Tan IIA on the NF-κB signaling pathway. TNF-α increased the normalized levels of NF-κB pathway-related proteins, including p-IKKα/β, p-IκB-α and p-NF-κB p65 (each normalized to its respective total protein), indicating activation of this signaling pathway (Fig. 6). Compared with the 0 μM group, Tan IIA at 10 μM significantly reduced the normalized levels of these proteins (p-IKKα/β, p-IκB-α and p-NF-κB p65). These results indicated that Tan IIA-mediated inhibition of expression of E-selectin and ICAM on HUVECs is associated with NF-κB signaling pathway.

Molecular docking predicted that Tan IIA can favorably bind to the extracellular domains of CD29(-9.976 kcal/mol) and P-selectin (-8.638 kcal/mol) with strong binding affinity (Fig. 7). The docking models suggested that Tan IIA

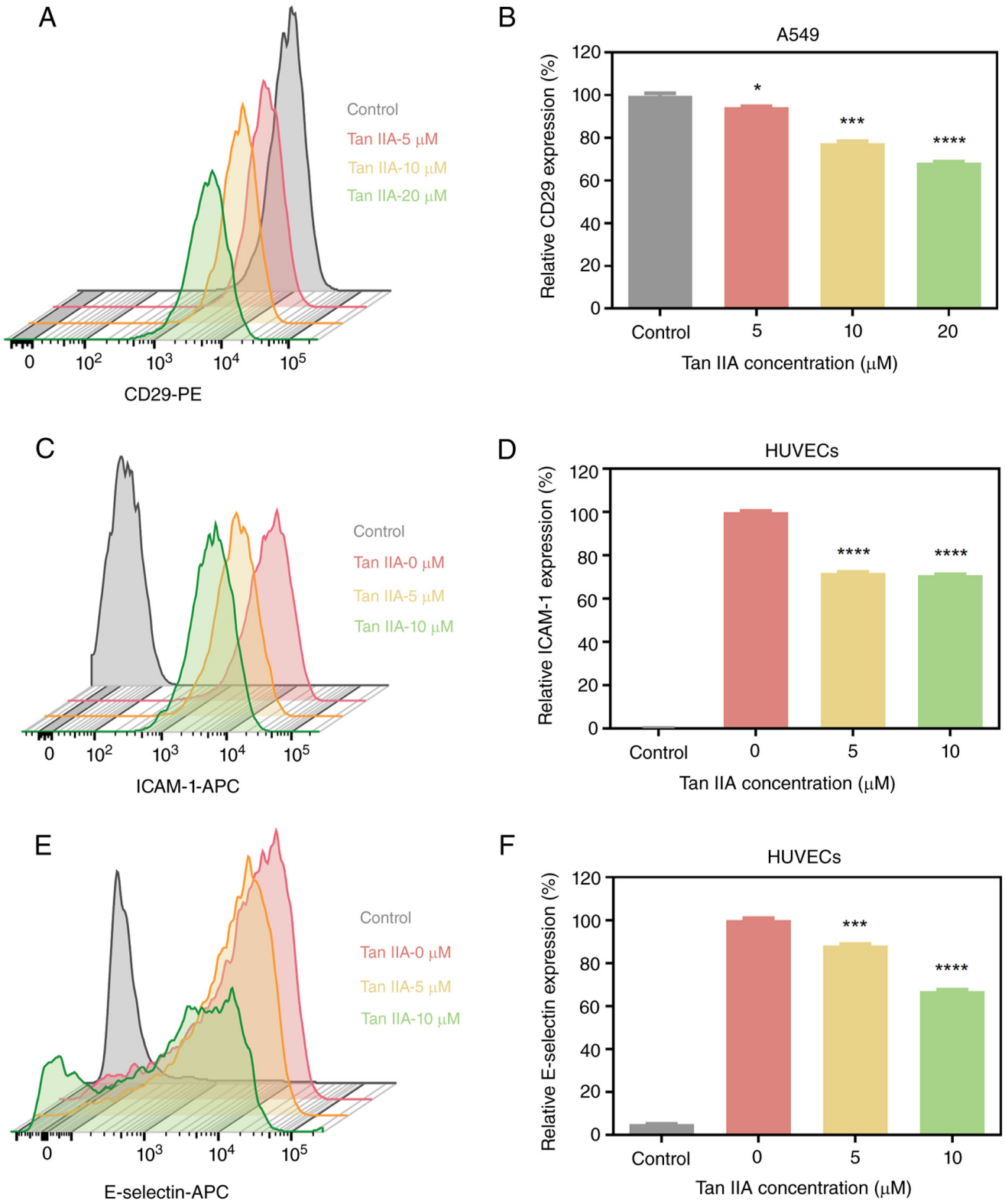

Figure 3. Regulation of adhesion molecule expression by Tan IIA. (A) Tan IIA significantly decreased the expression of CD29 on the surface of A549 cells, thereby decreasing tumor cell adhesive potential. (B) Quantitative results of the expression of CD29 on the surface of A549 cells. *P<0.05, ***P<0.001 and ****P<0.0001 vs. control (without Tan IIA). (C) Tan IIA attenuated the expression of ICAM-1 in HUVECs. (D) Quantitative results of ICAM-1 expression are shown. ****P<0.0001 vs. 0. (E) Tan IIA attenuated the expression of E-selectin in HUVECs. (F) Quantitative results of E-selectin expression are shown. These findings indicate that Tan IIA modulated both tumor cells and endothelial cells to create a less permissive metastatic microenvironment. ***P<0.001 and ****P<0.0001 vs. 0. Tan IIA, tanshinone IIA; ICAM, intercellular adhesion molecule; HUVEC, human umbilical vein endothelial cells.

potentially binds key functional regions or pockets on these proteins, which may interfere with their inter-molecular interactions.

Tan IIA inhibits metastatic progression and improves outcomes in vivo. To evaluate the anti-metastatic effects of Tan IIA *in vivo*, mouse models were established. In the A549

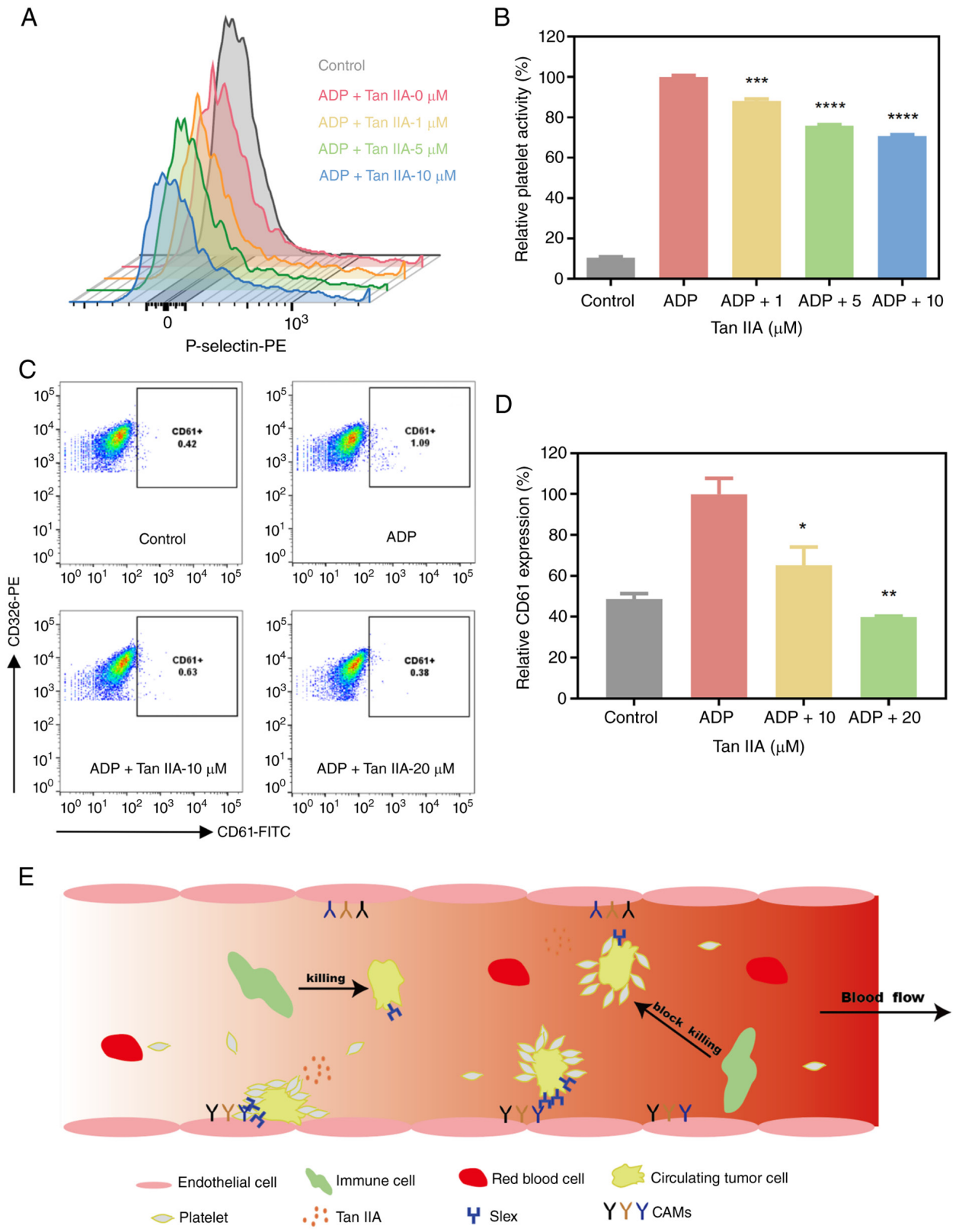

Figure 4. Effects of Tan IIA on platelet activation and tumor cell-platelet aggregation. (A) Tan IIA significantly inhibited platelet activation, as indicated by reduced expression of the platelet activation marker P-selectin. (B) Quantitative results of platelet activity. (C) Flow cytometric detection of tumor cell-platelet aggregation. (D) Quantitative results showed that Tan IIA markedly decreased the formation of platelet-tumor cell aggregates. *P<0.05, **P<0.01, ***P<0.001 and ****P<0.0001 vs. ADP. (E) Schematic of the inhibitory effects of Tan IIA on platelet-mediated interactions within the circulating tumor cells microenvironment. Tumor cell surface antigen sLex is recognized by P-selectin receptors on platelets, forming platelet-tumor cell aggregates, which protect tumor cells from immune recognition and attack. Following Tan IIA treatment, the expression of P-selectin on platelets is decreased, leading to disruption of platelet-tumor cell aggregates and partial or complete exposure of tumor cells to the immune system. Binding of tumor cell surface antigen sLex to selectins on endothelial cells increases adhesion, and Tan IIA can also inhibit this process by suppressing E-selectin expression on endothelial cells. Tan IIA can inhibit the adhesion of tumor cells to endothelial cells by decreasing expression of ICAM-1 on the endothelial cell surface and CD29 on the tumor cell surface, a process that depends on the binding of ICAM-1/VCAM between tumor and endothelial cells. Tan IIA, tanshinone IIA; sLex, sialyl Lewis X; ICAM, intercellular adhesion molecule; VCAM, vascular cell adhesion molecule.

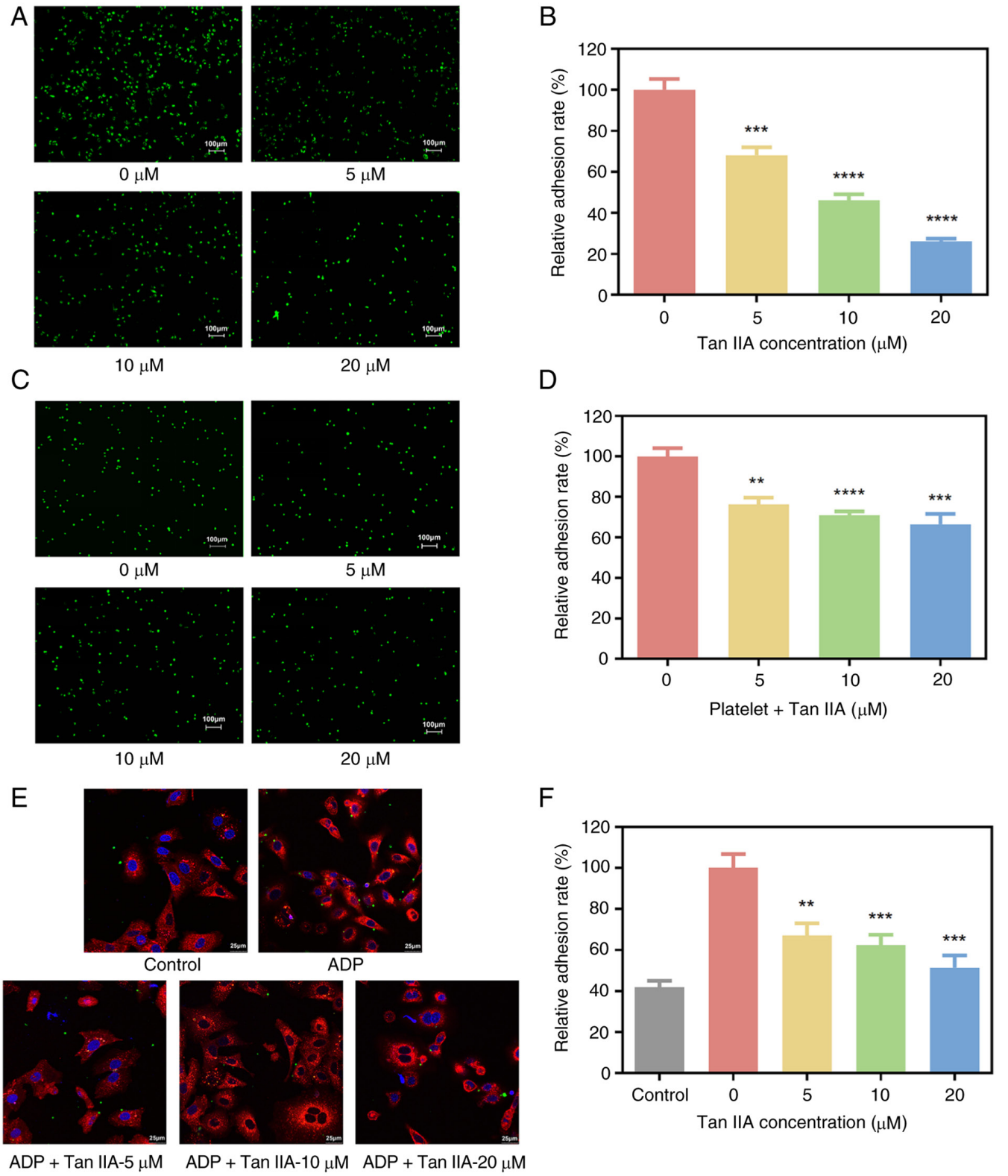

Figure 5. Tan IIA inhibits adhesion of tumor to endothelial cells. (A) Tan IIA significantly decreased the adhesion of A549 cells (green, Rhodamine-123-labeled) to TNF-α-stimulated HUVECs without platelet activation, (B) as quantified. (C) Tan IIA significantly decreased the adhesion of A549 cells to TNF-α-stimulated HUVECs in the presence of platelet activation, (D) as quantified. (E) Confocal microscopy confirmed that Tan IIA decreased platelet attachment to the surface of tumor cells. A549 cells were labeled with PKH26 (red), platelets were labeled with CFSE (green) and the cell nucleus was labeled with DAPI (blue). (F) Quantification of the effect of Tan IIA on platelet adhesion to the tumor cell surface. **P<0.01, ***P<0.001 and ****P<0.0001 vs. 0. Tan IIA, tanshinone IIA; CFSE, carboxyfluorescein diacetate N-succinimidyl ester; HUVEC, human umbilical vein endothelial cells.

tail vein metastasis model, Tan IIA significantly prolonged survival compared with controls (P=0.0169; Fig. 8A), but no significant body weight loss was observed during treatment (Fig. 8B). The number of lung metastatic nodules was significantly decreased in Tan IIA-treated mice, particularly in the 50 mg/kg/day group (Fig. 8C).

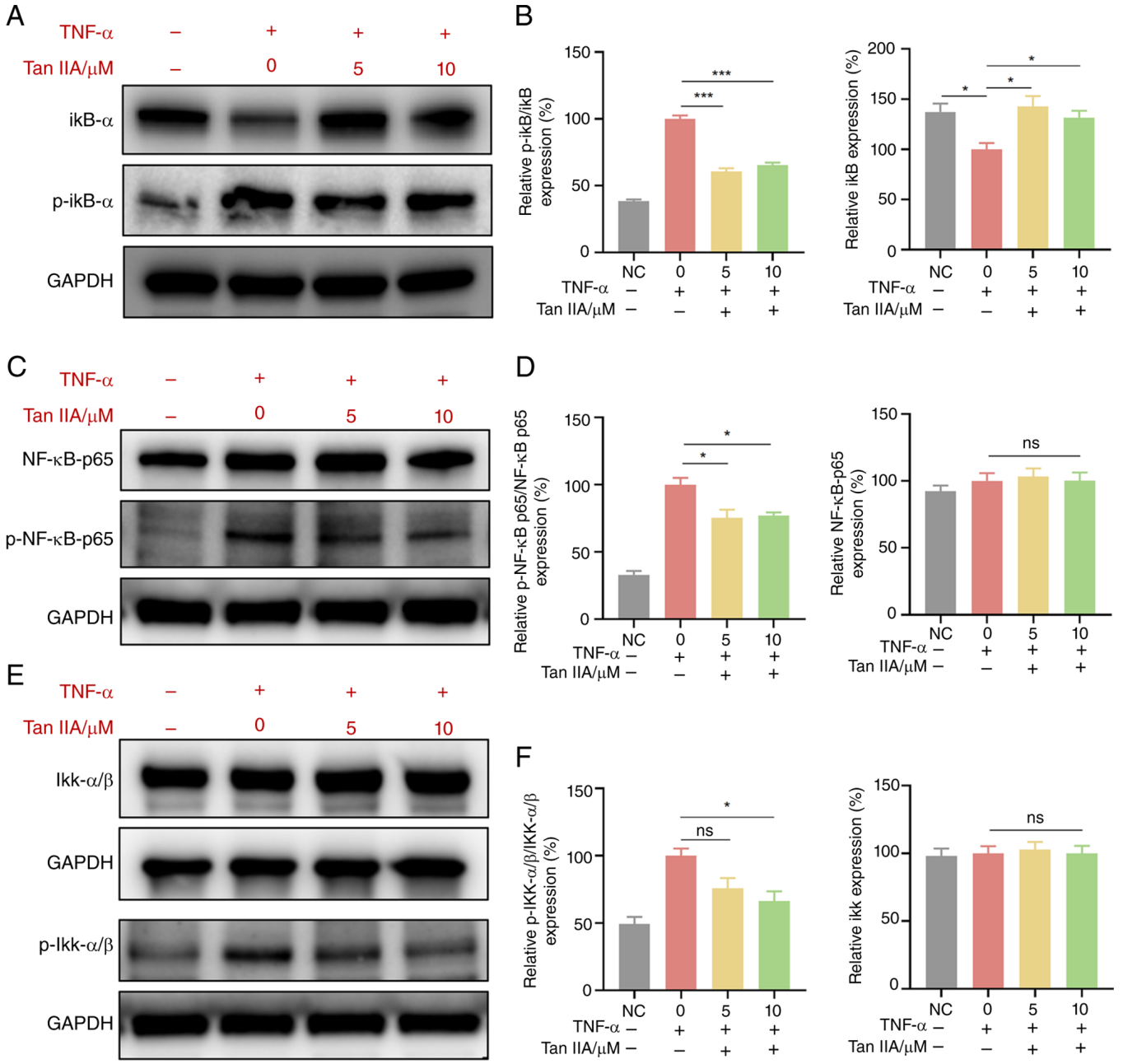

Figure 6. Tan IIA inhibits the NF-κB signaling pathway in HUVECs. (A) Protein expression levels of IκB-α and p-IκB-α in HUVECs were determined by western blotting at 24 h after treatment. (B) Quantification of p-IκB-α normalized to total IκB-α is shown. (C) Protein expression levels of NF-κB p65 and p-NF-κB p65 in HUVECs were determined by western blotting at 24 h after treatment. (D) Quantification of p-NF-κB p65 normalized to total NF-κB p65 is shown. (E) Protein expression levels of IKK-α/β and p-IKK-α/β in HUVECs were determined by western blotting at 24 h after treatment. (F) Quantification of p-IKK-α/β normalized to total IKK-α/β is shown. *P<0.05, ***P<0.001 vs. 0. Tan IIA, tanshinone IIA; p-, phosphorylated; HUVECs, human umbilical vein endothelial cells; ns, not significant; NC, negative control.

Consistent results were observed in both 4T1 models. In the hematogenous model, Tan IIA significantly decreased the number of lung metastases (Fig. 8D and E). Similarly, in the orthotopic model, Tan IIA led to fewer lung metastatic nodules compared with controls (Fig. 8G and H). Lung weight was largely unchanged across groups (Fig. 8F and I) and no significant body weight loss was observed during treatment (Fig. 8J and K), indicating good tolerability. Taken together, these *in vivo* findings demonstrated that Tan IIA effectively suppressed metastatic tumor burden while improving overall physiological condition and survival.

Discussion

Among 1,030,937 US (1992-2019) metastatic cancer survivors, 82.6% died from their metastatic cancer (highest in lung, pancreas, esophagus and stomach tumors) and 17.4% from competing causes (50). Metastasis poses clinical challenges such as therapeutic resistance, lesion heterogeneity and plasticity (51). The presence of CTCs in the bloodstream reflects the metastatic potential of malignant tumors and is associated with disease progression (52). In clinical practice, the number and biological characteristics of CTCs are

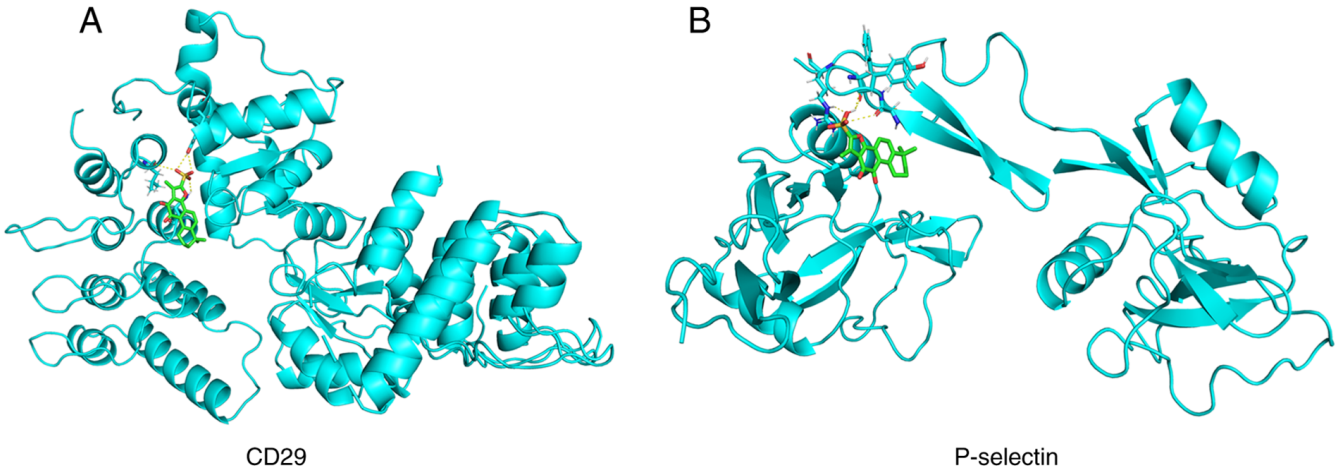

C

Program	CD29	P-selectin
REMARK VINA RESULT/(kcal/mol)	–9.172	–7.942
REMARK INTER + INTRA/(kcal/mol)	–9.955	–8.832
REMARK INTER/(kcal/mol)	–9.976	–8.638
REMARK INTRA/(kcal/mol)	0.021	–0.194

Figure 7. Molecular docking models and binding energies of Tan IIA with target proteins. Molecular docking models between Tan IIA and (A) CD29and (B) P-selectin. (C) Binding energies obtained using AutoDock Vina. Tan IIA, tanshinone IIA.

increasingly (53,54) recognized as valuable indicators for monitoring metastatic risk and therapeutic response (55). Because adhesion of CTCs to vascular endothelial cells is a key early event in hematogenous metastasis, strategies that eliminate CTCs or disrupt their adhesion and extravasation represent effective approaches to suppress metastatic spread (56). Studies have shown that the hematogenous microenvironment of CTCs, particularly platelet activation, platelet-tumor cell interactions and endothelial adhesion molecule expression, is a potential target for anti-metastatic intervention (57,58).

Traditional Chinese Medicine is characterized by multi-target actions and low toxicity and is widely applied as an adjunctive approach in cancer treatment, including metastatic disease (59,60). Tan IIA, a bioactive compound derived from *S. miltiorrhiza*, has demonstrated anti-tumor activity in multiple cancer types (61). Rather than exerting strong direct cytotoxic effects, Tan IIA exerts regulatory effects on vascular function, platelet activity and inflammatory responses (20). The present study therefore focused on the effects of Tan IIA at low, non-cytotoxic concentrations on metastasis-associated cellular interactions, specifically those among tumor cells, platelets and endothelial cells.

Once CTCs enter the circulation, they interact with platelets, resulting in platelet activation and the formation of tumor cell-platelet aggregates (57). Activated platelets express high levels of P-selectin, which mediates platelet adhesion to CTCs and contributes to platelet cloaking of CTCs. This cloaking protects tumor cells from hemodynamic shear stress and immune-mediated clearance and facilitates their arrest within the vasculature (62). Platelet activation and inflammatory stimulation promote endothelial activation, leading to increased expression of adhesion molecules such as E-selectin and ICAM-1 on endothelial cells (63). These molecules support tumor cell rolling, firm adhesion and stable attachment to the endothelial surface, which are prerequisites for transendothelial migration and metastatic colonization (64). Consistent with this metastatic cascade, the present results demonstrated that Tan IIA interferes with multiple steps of tumor dissemination. Tan IIA reduced the expression of CD29 on A549 cells, thereby weakening tumor cell adhesive capacity. Tan IIA inhibited platelet activation, as indicated by decreased P-selectin expression, and significantly decreased platelet adhesion to CTCs, limiting platelet cloaking. Moreover, Tan IIA attenuated TNF-α-induced upregulation of endothelial adhesion molecules ICAM-1 and E-selectin on HUVECs. These effects resulted in reduced tumor cell adhesion to endothelial cells and impaired platelet-mediated enhancement of tumor cell-endothelial interaction.

Endothelial cell activation and aberrantly high expression of adhesion molecules are key steps in the initiation of inflammatory responses, as well as in tumor cell adhesion and metastasis (65,66). The present study found that Tan IIA inhibited the upregulation of ICAM-1 and E-selectin in TNF-α-stimulated HUVEC cells. Tan IIA significantly decreased TNF-α-induced phosphorylation of IκBα, IKK-α/β and p65 (normalized to its respective total protein), indicating that Tan IIA inhibited adhesion molecule expression by blocking the canonical NF-κB pathway. This is consistent with anti-inflammatory effects of Tan IIA in other cell types (67,68). Furthermore, computational molecular docking

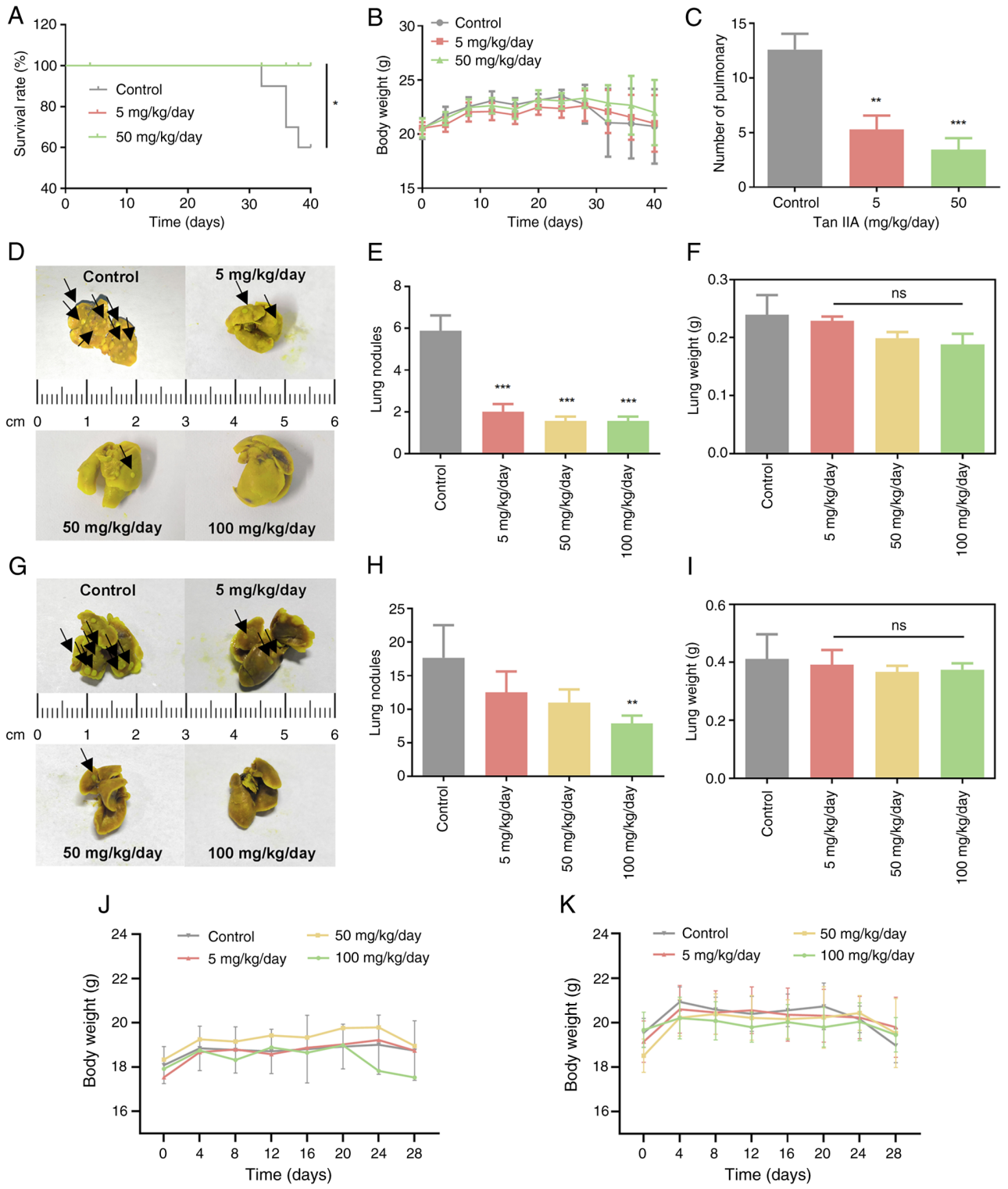

Figure 8. *In vivo* inhibition of cancer metastasis by Tan IIA. In the A549 tail vein metastasis model, Tan IIA (A) significantly prolonged survival compared with controls (P=0.0169), but (B) no significant body weight loss was observed during treatment. (C) Tan IIA decreased the number of metastatic lung nodules. In Balb/c mice injected intravenously with 4T1 cells, (D) gross view images of the lungs are shown. Statistical results showed that Tan IIA markedly (E) decreased pulmonary metastatic burden (F) without significantly affecting lung weight. Similar inhibitory effects on lung metastasis were observed in the orthotopic 4T1 mammary fat pad model. (G) Gross view images of the lungs are shown. Statistical results showed that high-concentration Tan IIA (100 mg/kg/day) also (H) markedly decreased pulmonary metastatic burden (I) without significantly affecting lung weight. No significant changes in body weight were observed in (J) the hematogenous model and (K) orthotopic 4T1 mammary fat pad model during treatment. Arrows indicate lung nodules. *P<0.05, **P<0.01, ***P<0.001 vs. control. Tan IIA, tanshinone IIA; ns, not significant.

predicted that Tan IIA can favorably bind to the extracellular domains of CD29 and P-selectin with strong binding affinity (binding energies <-6.8 kcal/mol). These results demonstrated that Tan IIA may exert its inhibitory effects, at least in part, through direct binding to these key adhesion molecules, potentially blocking their reciprocal interactions.

The present *in vitro* findings were supported by *in vivo* evidence from metastatic mouse models. Tan IIA decreased lung metastatic burden and prolonged survival in the A549 tail vein model, while also suppressing pulmonary metastasis in both tail vein and orthotopic 4T1 breast cancer models. Notably, these anti-metastatic effects occurred without significant changes in body or lung weight, suggesting that Tan IIA exerted its effects primarily through modulation of metastatic processes rather than overt toxicity. The concentrations of Tan IIA (5-20 μM) used to inhibit platelet activation, endothelial adhesion and tumor cell adhesion were selected based on prior mechanistic studies (33,69,70). While direct measurement of plasma concentrations in the present mouse model was not performed, pharmacokinetics data provide a relevant context. For example, oral administration of 4.1 mg/kg Tan IIA in rats results in a maximum concentration of 2.78±0.96 ng/ml (~8.7 nM) and an area under the curve of 4.53 ng·h/ml (71). The effective concentrations *in vitro* are therefore higher than reported systemic plasma levels. This is a common scenario for natural compounds where *in vitro* mechanistic studies employ concentrations that may not reflect systemic bioavailability but are justified to elucidate potential targets and pathways (72). Effective anti-metastatic concentrations may result in significantly higher local concentrations in key tissue such as the lung or liver due to tissue distribution and accumulation, as suggested for other lipophilic compounds (73,74). Furthermore, the primary metabolite of Tan IIA, tanshinol, may also contribute to the overall biological activity (75,76). Future studies measuring tissue-specific pharmacokinetics and the activity of notable metabolites are warranted to bridge this gap and optimize dosing strategies.

The present study had limitations. First, while the present study demonstrates a clear association between Tan IIA treatment and decreased tumor cell-platelet-endothelial interactions, the precise upstream molecular targets of Tan IIA were not fully delineated and did not formally establish that this axis is the primary mediator of the observed reduction in pulmonary metastasis. Future studies employing conditional platelet depletion, tumor cells with genetic ablation of specific adhesion receptors (CD29) or neutralizing antibodies against key interaction molecules (P-selectin) in metastatic models are required to validate the causal role of the disrupted adhesion cascade. Second, while HUVECs are a well-established and accessible model for studies of endothelial behavior, organ-specific microvascular endothelial cells (such as from the lung) may differ in their response to stimuli (77-79). Future studies employing lung microvascular endothelial cells are required to validate the translational relevance of the present findings to pulmonary metastasis. Finally, although the *in vivo* models provided support for an anti-metastatic role of Tan IIA, additional pharmacokinetic and dose-response studies are necessary to facilitate clinical translation.

Taken together, the present findings supported the hypothesis that Tan IIA suppresses hematogenous metastasis primarily by modulating interactions between CTCs, platelets and endothelial cells. Tan IIA may do this by attenuating platelet activation, decreasing tumor cell-platelet aggregation and limiting tumor cell adhesion to the vascular endothelium, and inhibiting the NF-κB signaling pathway that leads to adhesion protein expression in vascular endothelial cells. Tan IIA disrupts key early steps of metastatic dissemination. The present results highlight Tan IIA as a potential pharmacological agent targeting the metastatic microenvironment rather than tumor cell viability.

Acknowledgements

Not applicable.

Funding

The present study was supported by the National Natural Science Foundation of China (grant nos. 81703555 and 81961138017), the Department of Science and Technology of Fujian Province (grant nos. 2025I0051, 2023Y9124 and 2021D043) and the Research Project of Fashu Foundation (grant no. MFK24021).

Availability of data and materials

The data generated in the present study may be requested from the corresponding author.

Authors' contributions

JX analyzed data, designed and performed experiments, constructed figures and wrote the manuscript. LL analyzed data, designed and performed experiments and wrote the manuscript. FL analyzed data, designed and performed experiments and edited the manuscript. SW analyzed data, designed and performed experiments and supervised the study. CF designed the study. GW designed and performed experiments and constructed figures. YW and YL conceived the study and edited the manuscript. YL analyzed data, constructed figures, supervised the study and edited the manuscript. JX and FL confirm the authenticity of all the raw data. All authors have read and approved the final manuscript.

Ethics approval and consent to participate

The animal study was reviewed and approved by the institutional animal care and use committee of Minjiang University, Fuzhou, China (approval no. IACUC-MJLAC-2023-020). The collection and use of human blood samples in this study was reviewed and approved by the Ethics Committee of Fujian Medical University Union Hospital, Fuzhou, China (approval no. 2022KJT046). All patients provided written informed consent to participate.

Patient consent for publication

Not applicable.

Competing interests

The authors declare that they have no competing interests.

References

1. Garemilla SSS, Kadambala MC, Gampa SC, Chinthala S and Garimella SV: Cancer metastasis: Therapeutic challenges and opportunities. Med Oncol 42: 518, 2025.
2. Steeg PS: Tumor metastasis: Mechanistic insights and clinical challenges. Nat Med 12: 895-904, 2006.
3. Shen MM: Cancer: The complex seeds of metastasis. Nature 520: 298-299, 2015.
4. Lu Y, Lian S, Ye Y, Yu T, Liang H, Cheng Y, Xie J, Zhu Y, Xie X, Yu S, *et al*: S-Nitrosocaptopril prevents cancer metastasis in vivo by creating the hostile bloodstream microenvironment against circulating tumor cells. Pharmacol Res 139: 535-549, 2019.
5. Lu Y, Liang H, Yu T, Xie J, Chen S, Dong H, Sinko PJ, Lian S, Xu J, Wang J, *et al*: Isolation and characterization of living circulating tumor cells in patients by immunomagnetic negative enrichment coupled with flow cytometry. Cancer 121: 3036-3045, 2015.
6. Zhou L, Zhang Z, Tian Y, Li Z, Liu Z and Zhu S: The critical role of platelet in cancer progression and metastasis. Eur J Med Res 28: 385, 2023.
7. Morris K, Schnoor B and Papa AL: Platelet cancer cell interplay as a new therapeutic target. Biochim Biophys Acta Rev Cancer 1877: 188770, 2022.
8. Rejniak KA: Circulating tumor cells: When a solid tumor meets a fluid microenvironment. Adv Exp Med Biol 936: 93-106, 2016.
9. Kong DH, Kim YK, Kim MR, Jang JH and Lee S: Emerging roles of vascular cell adhesion Molecule-1 (VCAM-1) in immunological disorders and cancer. Int J Mol Sci 19: 1057, 2018.
10. Lu Y, Lian S, Cheng Y, Ye Y, Xie X, Fu C, Zhang C, Zhu Y, Iqbal Parker M and Jia L: Circulation patterns and seed-soil compatibility factors cooperate to cause cancer organ-specific metastasis. Exp Cell Res 375: 62-72, 2019.
11. Wei B, Sun C, Wan H, Shou Q, Han B, Sheng M, Li L and Kai G: Bioactive components and molecular mechanisms of *Salvia miltiorrhiza* Bunge in promoting blood circulation to remove blood stasis. J Ethnopharmacol 317: 116697, 2023.
12. Li Y, Liao J, Xiong L, Xiao Z, Ye F, Wang Y, Chen T, Huang L, Chen M, Chen ZS, *et al*: Stepwise targeted strategies for improving neurological function by inhibiting oxidative stress levels and inflammation following ischemic stroke. J Control Release 368: 607-622, 2024.
13. Su CY, Ming QL, Rahman K, Han T and Qin LP: *Salvia miltiorrhiza*: Traditional medicinal uses, chemistry, and pharmacology. Chin J Nat Med 13: 163-182, 2015.
14. Zhang W, Feng J, Liu R, Xiang T and Wu X: Tanshinone IIA regulates NRF2/NLRP3 signal pathway to restrain oxidative stress and inflammation in Uric Acid-induced HK-2 fibrotic models. Endocr Metab Immune Disord Drug Targets 25: 721-731, 2024.
15. Hu CH, Chen Y, Jin TY, Wang Z, Jin B, Liao J, Ding CY, Zhang A, Tang WY, Zhang LX, *et al*: A derivative of tanshinone IIA and salviadione, 15a, inhibits inflammation and alleviates DSS-induced colitis in mice by direct binding and inhibition of RIPK2. Acta Pharmacol Sin 46: 672-686, 2025.
16. Liu Q, Li X and Luo Y: Tanshinone IIA delays liver aging by modulating oxidative stress. Front Pharmacol 15: 1434024, 2024.
17. Li Y, Guo Z, Li P, Guo J, Wang H, Pan W, Wu F, Li J, Zhou J and Ma Z: Tanshinone T1/T2A inhibits non-small cell lung cancer through Lin28B-let-7-BORA/MYC regulatory network. Gene 935: 149058, 2024.
18. Fang ZY, Zhang M, Liu JN, Zhao X, Zhang YQ and Fang L: Tanshinone IIA: A review of its anticancer effects. Front Pharmacol 11: 611087, 2020.
19. Zhang W, Feng J, Liu R, Xiang T and Wu X: Tanshinone IIA regulates NRF2/NLRP3 signal pathway to restrain oxidative stress and inflammation in uric acid-induced HK-2 fibrotic models. Endocr Metab Immune Disord Drug Targets 25: 721-731, 2025.
20. Zhu T, Chen J, Zhang M, Tang Z, Tong J, Hao X, Li H, Xu J and Yang J: Tanshinone IIA exerts cardioprotective effects through improving Gut-Brain axis post-myocardial infarction. Cardiovasc Toxicol 24: 1317-1334, 2024.
21. Mao D, Wang H, Guo H, Che X, Chen M, Li X, Liu Y, Huo J and Chen Y: Tanshinone IIA normalized hepatocellular carcinoma vessels and enhanced PD-1 inhibitor efficacy by inhibiting ELTD1. Phytomedicine 123: 155191, 2024.
22. Wang P, Gu Y, Lu J, Song M, Hou W, Li P, Sun Y, Wang J and Chen X: Endothelial TRPV4 channel mediates the vasodilation induced by Tanshinone IIA. Chem Biol Interact 402: 111181, 2024.
23. Liu HH, Wei W, Wu FF, Cao L, Yang BJ, Fu JN, Li JX, Liang XY, Dong HY, Heng YY and Zhang PF: Sodium tanshinone IIA sulfonate protects vascular relaxation in ApoE-knockout mice by inhibiting the SYK-NLRP3 inflammasome-MMP2/9 pathway. BMC Cardiovasc Disord 24: 354, 2024.
24. Zhang Y, Xin G, Zhou Q, Yu X, Feng L, Wen A, Zhang K, Wen T, Zhou X, Wu Q, *et al*: Elucidating the distinctive regulatory effects and mechanisms of active compounds in *Salvia miltiorrhiza* Bunge via network pharmacology: Unveiling their roles in the modulation of platelet activation and thrombus formation. Toxicol Appl Pharmacol 484: 116871, 2024.
25. Yu JR, Liu YY, Gao YY, Qian LH, Qiu JL, Wang PP and Zhang GJ: Diterpenoid tanshinones inhibit gastric cancer angiogenesis through the PI3K/Akt/mTOR signaling pathway. J Ethnopharmacol 324: 117791, 2024.
26. Xuan Y, Yu C, Ni K, Congcong L, Lixin Q and Qingxian L: Protective effects of tanshinone IIA on Porphyromonas gingivalis-induced atherosclerosis via the downregulation of the NOX2/NOX4-ROS mediation of NF-κB signaling pathway. Microbes Infect 25: 105177, 2023.
27. Zeng JY, Wang Y, Hong FY, Miao M, Jiang YY, Qiao ZX, Wang YT and Bao XR: Tanshinone IIA is superior to paricalcitol in ameliorating tubulointerstitial fibrosis through regulation of VDR/Wnt/β-catenin pathway in rats with diabetic nephropathy. Naunyn Schmiedebergs Arch Pharmacol 397: 3959-3977, 2024.
28. Wei W, Heng YY, Wu FF, Dong HY, Zhang PF, Li JX, Liu CY, Yang BJ, Fu JN and Liang XY: Sodium Tanshinone IIA Sulfonate alleviates vascular senescence in diabetic mice by modulating the A20-NFκB-NLRP3 inflammasome-catalase pathway. Sci Rep 14: 17665, 2024.
29. Li H, Hu P, Zou Y, Yuan L, Xu Y, Zhang X, Luo X and Zhang Z: Tanshinone IIA and hepatocellular carcinoma: A potential therapeutic drug. Front Oncol 13: 1071415, 2023.
30. Zhang P, Liu W and Wang Y: The mechanisms of tanshinone in the treatment of tumors. Front Pharmacol 14: 1282203, 2023.
31. Liang EY, Huang MH, Chen YT, Zhang PW, Shen Y, Tu XX, Chen WY, Wang Y, Yan J, Wang HY, *et al*: Tanshinone IIA modulates cancer cell morphology and movement via Rho GTPases-mediated actin cytoskeleton remodeling. Toxicol Appl Pharmacol 483: 116839, 2024.
32. Jiang Y, Bi Y, Zhou L, Zheng S, Jian T and Chen J: Tanshinone IIA inhibits proliferation and migration by downregulation of the PI3K/Akt pathway in small cell lung cancer cells. BMC Complement Med Ther 24: 68, 2024.
33. Ge T, Li H, Xiang P, Yang D, Zhou J and Zhang Y: Tanshinone IIA induces ferroptosis in colorectal cancer cells through the suppression of SLC7A11 expression via the PI3K/AKT/mTOR pathway. Eur J Med Res 30: 576, 2025.
34. Ji XZ, Qin X, Wang W and Wang L: A review of tanshinone compounds in prostate cancer treatment. Transl Androl Urol 13: 1278-1287, 2024.
35. Liu L, Gao H, Wen T, Gu T, Zhang S and Yuan Z: Tanshinone IIA attenuates AOM/DSS-induced colorectal tumorigenesis in mice via inhibition of intestinal inflammation. Pharm Biol 59: 89-96, 2021.
36. Qian J, Cao Y, Zhang J, Li L, Wu J, Wei G, Yu J and Huo J: Tanshinone IIA induces autophagy in colon cancer cells through MEK/ERK/mTOR pathway. Transl Cancer Res 9: 6919-6928, 2020.
37. Ma S, Lei Y, Zhang L and Wang J: Research on the inhibiting effect of tanshinone IIA on colon cancer cell growth via COX-2-Wnt/β-catenin signaling pathway. J BUON 23: 1337-1342, 2018.
38. Lu Y, Yu T, Liang H, Wang J, Xie J, Shao J, Gao Y, Yu S, Chen S, Wang L and Jia L: Nitric oxide inhibits hetero-adhesion of cancer cells to endothelial cells: Restraining circulating tumor cells from initiating metastatic cascade. Sci Rep 4: 4344, 2014.
39. Petpiroon N, Sritularak B and Chanvorachote P: Phoyunnanin E inhibits migration of non-small cell lung cancer cells via suppression of epithelial-to-mesenchymal transition and integrin αv and integrin β3. BMC Complement Altern Med 17: 553, 2017.
40. National Research Council Committee for the Update of the Guide for the C and Use of Laboratory A: The National Academies Collection: Reports funded by National Institutes of Health. In: Guide for the Care and Use of Laboratory Animals National Academies Press US, Copyright© 2011, National Academy of Sciences, Washington, DC, 2011.

41. Alessio M, Petiti J, Basile R, Poggio P, Acquarone D, Scalera A, Avalle L, Orso F, Bertoni A, Porporato PE, *et al*: Mitochondrial IκBα fuels cancer progression through metabolic rewiring, endothelial activation, and thrombotic spread. Cell Death Discov: Mar 27, 2026 (Epub ahead of print). doi: 10.1038/s41420-026-03022-0.
42. Rab SO, Altalbawy FMA, Bishoyi AK, Ballal S, Kareem M, Singh A, Kubaev A, Soleimani Samarkhazan H and Bagheri S: Targeting platelet-tumor cell interactions: A novel approach to cancer therapy. Medical Oncology 42: 232, 2025.
43. Souchak J, Mohammed NBB, Lau LS and Dimitroff CJ: The role of galectins in mediating the adhesion of circulating cells to vascular endothelium. Front Immunol 15: 1395714, 2024.
44. Jung SM and Moroi M: Activation of the platelet collagen receptor integrin alpha(2)beta(1): Its mechanism and participation in the physiological functions of platelets. Trends Cardiovasc Med 10: 285-292, 2000.
45. Chen Y, Yang S, Tavormina J, Tampe D, Zeisberg M, Wang H, Mahadevan KK, Wu CJ, Sugimoto H, Chang CC, *et al*: Oncogenic collagen I homotrimers from cancer cells bind to α3β1 integrin and impact tumor microbiome and immunity to promote pancreatic cancer. Cancer Cell 40: 818-834.e9, 2022.
46. Chriqui LE, Cavin S and Perentes JY: Dual implication of endothelial adhesion molecules in tumor progression and cancer immunity. Cell Adh Migr 19: 2472308, 2025.
47. Labelle M and Hynes RO: The initial hours of metastasis: The importance of cooperative host-tumor cell interactions during hematogenous dissemination. Cancer Discov 2: 1091-1099, 2012.
48. Geng JG, Chen M and Chou KC: P-selectin cell adhesion molecule in inflammation, thrombosis, cancer growth and metastasis. Curr Med Chem 11: 2153-2160, 2004.
49. Barbazán J, Alonso-Alconada L, Elkhatib N, Geraldo S, Gurchenkov V, Glentis A, van Niel G, Palmulli R, Fernández B, Viaño P, *et al*: Liver metastasis is facilitated by the adherence of circulating tumor cells to vascular fibronectin deposits. Cancer Res 77: 3431-3441, 2017.
50. Mani K, Deng D, Lin C, Wang M, Hsu ML and Zaorsky NG: Causes of death among people living with metastatic cancer. Nat Commun 15: 1519, 2024.
51. Ma B, Wells A and Clark AM: The pan-therapeutic resistance of disseminated tumor cells: Role of phenotypic plasticity and the metastatic microenvironment. Semin Cancer Biol 60: 138-147, 2020.
52. Lawrence R, Watters M, Davies CR, Pantel K and Lu YJ: Circulating tumour cells for early detection of clinically relevant cancer. Nat Rev Clin Oncol 20: 487-500, 2023.
53. Jiang L, Yang H, Cheng W, Ni Z and Xiang N: Droplet microfluidics for CTC-based liquid biopsy: A review. Analyst 148: 203-221, 2023.
54. Alix-Panabières C, Marchetti D and Lang JE: Liquid biopsy: From concept to clinical application. Sci Rep 13: 21685, 2023.
55. Castro-Giner F and Aceto N: Tracking cancer progression: From circulating tumor cells to metastasis. Genome Med 12: 31, 2020.
56. Chen S, Yang X, Zhang Y, Liu Y, Lu H, Qiu Y, Cheng L, Li C and Wang C: Inhalable porous microspheres loaded with metformin and docosahexaenoic acid suppress tumor metastasis by modulating premetastatic niche. Mol Pharm 18: 2622-2633, 2021.
57. Liu Y, Zhang Y, Ding Y and Zhuang R: Platelet-mediated tumor metastasis mechanism and the role of cell adhesion molecules. Crit Rev Oncol Hematol 167: 103502, 2021.
58. Reymond N, d'Água BB and Ridley AJ: Crossing the endothelial barrier during metastasis. Nat Rev Cancer 13: 858-870, 2013.
59. Shi XY, Bao X, Li Y and Yin CL: Theanine combined with cisplatin inhibits the proliferation and metastasis of TNBC cells through Akt signaling pathway. Tradit Med Res 8: 25-30, 2023.
60. Wang SF, Dong SQ, Dong Q, Lin WX, Dong M and Liu D: Natural product-induced oxidative stress-synergistic anti-tumor effects of chemotherapeutic agents. Tradit Med Res 9: 13-18, 2024.
61. Zhang W, Liu C, Li J, Lu Y, Li H, Zhuang J, Ren X, Wang M and Sun C: Tanshinone IIA: New perspective on the Anti-Tumor mechanism of A Traditional Natural Medicine. Am J Chin Med 50: 209-239, 2022.
62. Luo G, Jin K, Deng S, Cheng H, Fan Z, Gong Y, Qian Y, Huang Q, Ni Q, Liu C and Yu X: Roles of CA19-9 in pancreatic cancer: Biomarker, predictor and promoter. Biochim Biophys Acta Rev Cancer 1875: 188409, 2021.
63. Schmidt EP, Kuebler WM, Lee WL and Downey GP: Adhesion molecules: Master controllers of the circulatory system. Compr Physiol 6: 945-973, 2016.
64. Osmani N, Follain G, García León MJ, Lefebvre O, Busnelli I, Larnicol A, Harlepp S and Goetz JG: Metastatic tumor cells exploit their adhesion repertoire to counteract shear forces during intravascular arrest. Cell Rep 28: 2491-2500.e5, 2019.
65. Maltseva D, Nersisyan A and Tonevitsky A: Interplay of integrins and selectins in metastasis. Mol Oncol 19: 1582-1611, 2025.
66. Wang K, Dong S, Higazy D, Jin L, Zou Q, Chen H, Inayat A, Hu S and Cui M: Inflammatory environment promotes the adhesion of tumor cells to brain microvascular endothelial cells. Front Oncol 11: 691771, 2021.
67. Zhang Y, Wang J, Yang S, Kou H and Liu P: Tanshinone IIA alleviate atherosclerosis and hepatic steatosis via down-regulation of MAPKs/NF-κB signaling pathway. Int Immunopharmacol 152: 114465, 2025.
68. Zhou C, Yu Z, Chen T, Chen Q, Zhang Y, Cai J, Xu C and Yu L: Tanshinone IIA attenuates cerebral-ischemia-reperfusion-induced neuroinflammation by inhibiting the TLR4/NF-κB signaling cascade: A study integrating network pharmacology, bioinformatics, and experimental validation. Phytomedicine 149: 157548, 2025.
69. Chen H, Shu H, Su W, Li B, Zhang H, Li L, Lin C, Yi W, Zhan XY, Chen C, *et al*: Tanshinone IIA has a potential therapeutic effect on kawasaki disease and suppresses megakaryocytes in rabbits with immune vasculitis. Front Cardiovasc Med 9: 873851, 2022.
70. Fang J, Chen Q, He B, Cai J, Yao Y, Cai Y, Xu S, Rengasamy KRR, Gowrishankar S, Pandian SK and Cao T: Tanshinone IIA attenuates TNF-α induced PTX3 expression and monocyte adhesion to endothelial cells through the p38/NF-κB pathway. Food Chem Toxicol 121: 622-630, 2018.
71. Park EJ, Ji HY, Kim NJ, Song WY, Kim YH, Kim YC, Sohn DH and Lee HS: Simultaneous determination of tanshinone I, dihydrotanshinone I, tanshinone IIA and cryptotanshinone in rat plasma by liquid chromatography-tandem mass spectrometry: Application to a pharmacokinetic study of a standardized fraction of *Salvia miltiorrhiza*, PF2401-SF. Biomed Chromatogr 22: 548-555, 2008.
72. Lyu C, Zhang Y, Zhou W, Zhang S, Kou F, Wei H, Zhang N and Zuo Z: Gender-Dependent pharmacokinetics of veratramine in rats: In vivo and in vitro evidence. AAPS J 18: 432-444, 2016.
73. Liu Y, Wang L, Li X, Lv C, Feng D and Luo Z: Tanshinone IIA improves impaired nerve functions in experimental diabetic rats. Biochem Biophys Res Commun 399: 49-54, 2010.
74. Li F, Han G and Wu K: Tanshinone IIA alleviates the AD phenotypes in APP and PS1 transgenic mice. Biomed Res Int 2016: 7631801, 2016.
75. Jia W, Du F, Liu X, Jiang R, Xu F, Yang J, Li L, Wang F, Olaleye OE, Dong J and Li C: Renal tubular secretion of tanshinol: Molecular mechanisms, impact on its systemic exposure, and propensity for dose-related nephrotoxicity and for renal herb-drug interactions. Drug Metab Dispos 43: 669-678, 2015.
76. Zhu P, Liu Z, Zhou J and Chen Y: Tanshinol inhibits the growth, migration and invasion of hepatocellular carcinoma cells via regulating the PI3K-AKT signaling pathway. Onco Targets Ther 12: 87-99, 2019.
77. Urbanczyk M, Abuhelou A, Köninger M, Jeyagaran A, Carvajal-Berrio D, Kim E, Marzi J, Loskill P, Layland SL and Schenke-Layland K: Heterogeneity of endothelial cells impacts the functionality of human pancreatic in vitro models. Tissue Eng Part A 31: 988-1004, 2025.
78. Hennigs JK, Matuszcak C, Trepel M and Körbelin J: Vascular endothelial cells: Heterogeneity and targeting approaches. Cells 10: 2712, 2021.
79. Uwamori H, Ono Y, Yamashita T, Arai K and Sudo R: Comparison of organ-specific endothelial cells in terms of microvascular formation and endothelial barrier functions. Microvasc Res 122: 60-70, 2019.